Hindawi
Journal of Nanomaterials
Volume 2020, Article ID 3863428, 13 pages
https://doi.org/10.1155/2020/3863428

Research Article

Printability Optimization of Gelatin-Alginate Bioinks by Cellulose Nanofiber Modification for Potential Meniscus Bioprinting

Wenbin Luo,[1] **Zhengyi Song**,[2] **Zhonghan Wang**,[1] **Zhenguo Wang**,[2] **Zuhao Li**,[1] **Chenyu Wang**,[1,3] **He Liu**,[1] **Qingping Liu**,[2] **and Jincheng Wang**[1]

[1]*Department of Orthopedics, The Second Hospital of Jilin University, Changchun 130041, China*
[2]*Key Laboratory of Bionic Engineering (Ministry of Education), Jilin University, Changchun 130022, China*
[3]*Department of Plastic and Cosmetic Surgery, The First Hospital of Jilin University, Changchun 130021, China*

Correspondence should be addressed to He Liu; heliu@jlu.edu.cn, Qingping Liu; liuqp@jlu.edu.cn, and Jincheng Wang; jinchengwang2015@gmail.com

Received 21 March 2020; Accepted 7 April 2020; Published 5 May 2020

Academic Editor: Hui-Qi Xie

Meniscal injury is more likely to cause a permanent alteration of the biomechanical and biological environment of the knee joint, mainly due to the morphological mismatch and substantial loss of meniscal tissues. Herein, to overcome this challenge, we developed an improved bioink with enhanced printability, while maintaining the biocompatibility of major cellular component of the meniscus, namely fibrochondrocytes. Firstly, cellulose nanofiber (CNF) was mixed with gelatin-alginate thermal-responsive bioinks to improve the printability. Afterward, individual-specific meniscal prototypes based on the 3D reconstruction of MRI data were bioprinted using our bioink. The rheological and printability properties of the bioinks were characterized to select proper bioink content and bioprinting parameters. And then, a series of biological characterizations of the bioprinted samples, such as cell viability, metabolic activity, and extracellular matrix accumulation, were carried out in vitro. The results indicated that superior rheological performance and printability of CNF-modified bioink were achieved, ensuring high-precision bioprinting of specific-designed meniscal prototype when compared with the non-CNF-containing counterparts. Meanwhile, biological tests indicated that fibrochondrocytes encapsulated within the CNF-modified bioink maintained long-term cellular viability as well as acceptable extracellular matrix accumulation. This study demonstrates that the CNF-modified bioink is in favor of the printing fidelity of specific meniscus by improved rheological properties, minimizing the mismatch between artificial meniscal implants and native knee joint tissues, thereby permitting the evolution of clinical therapeutic methods of meniscal reconstruction.

1. Introduction

The menisci are two semilunar fibrocartilage structures located at the medial and lateral surface of the tibial plateau, which play a vital role in stabilization, nourishment, and force distribution of the knee joint [1]. Unfortunately, menisci are commonly involved in acute knee injury and osteoarthritis, resulting in substantial loss of meniscal tissue and permanent alteration of the biomechanical and biological environment of the knee joint [2]. Generally, meniscal allografts are applied in clinical with acceptable long-term follow-up results [3]. However, like all other allograft transplantation treatments, meniscal allografts are limited to tissue resources and the potential risk of mismatch, immunoreactivity, and disease transmission [4].

Several tissue engineering scaffolds have been developed with encouraging progress in avoiding meniscal allografting-relevant complications [5]. However, the mismatch of meniscal defect size and baseline articular cartilage still exists, leading to worsening articular cartilage status and greater displacement during long-term follow-up [6]. It has been reported that 1/3 mismatch of the meniscus could result in a 65% increase in peak local contact stresses, significantly deteriorating the degenerative changes of the articular cartilage [7]. Thus, the patient-specific design meeting individuals' joint requirements has been a vital element to

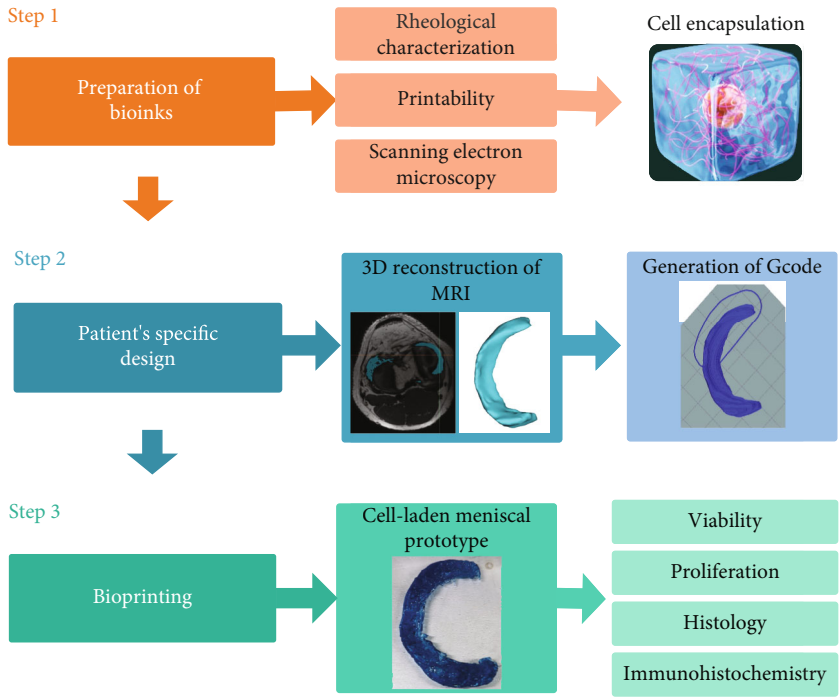

Scheme 1: Schematic representation of the study process.

improve the biological and biomechanical performances of tissue engineering meniscal scaffolds.

Bioprinting technology as a group of additive, bottom-up, nature-like technologies has made it possible to spatially pattern cells, bioactive factors, and biomaterials in the 3D microenvironment [8–11]. Bioprinting meniscal-shaped structures with stem cells or chondrocytes via microextrusion bioprinting technology as proof-of-concept tests have been reported [12, 13]. However, there are few meniscal bioprinting studies involving patient-specific design using major cellular components of the native meniscus with proper mechanically featured bioink until now.

Gelatin-alginate-based hydrogel has been widely applied as a bioink source in microextrusion approaches [14, 15]. As a hydrolytic product of collagen, gelatin can provide a favorite microenvironment enhancing cell attachment and proliferation, while alginate presents the feature of instant gelation via cross-linking by calcium ions (Ca^{2+}), enabling acceptable mechanical performance for bioprinted products [16]. Gelatin-alginate-based bioink systems present various advantages including widely available and economical material source, relatively simple producing process, and verified cytocompatibility [17]. Moreover, the thermal reversible feature of the gelatin-alginate-based bioink system enables a relatively simplified bioprinting process and device design [18]. However, during the microextrusion bioprinting process, the gelatin-alginate based hydrogels are fragile and changeable before further cross-linking, causing unstable mechanical condition especially in fabricating complex structures like the meniscus [19, 20].

Originating from the most abundant bioresource, wood biomass, cellulose nanofiber (CNF) is representative in building components in nature and has attracted significant interest as a potential biomaterial candidate [21]. In addition, CNF provides acceptable mechanical properties, relatively good rheological properties, and most importantly, cytocompatibility [22, 23]. However, to our knowledge, there has been no report of adapting CNF to improve the printability of alginate-gelatin-based bioink systems via hydrophobic interactions and hydrogen bonding for individual-specific meniscus biofabrication.

In this study, CNF was mixed with gelatin-alginate thermal-responsive bioinks to improve the printability. The rheological and morphological properties of the bioinks were characterized. While cell-laden meniscal prototype basing on MRI data was bioprinted using our CNF-modified bioinks, subsequently, the bioprinted prototypes underwent histological and immunohistochemical assessments to verify biological potentials as presented in Scheme 1. The current work aims at carrying out the preliminary practice on bioprinting implant prototype of patients' specific-designed, cell-laden products for potential meniscus transplantation.

2. Materials and Methods

2.1. Materials. The bioprinter (BioPrinter-1, BP-1) used in the current study was developed by our research group. Gelatin type B from bovine skin (G8061) and Na-alginate (A9640) were purchased from Solarbio Inc. (China). Wood-based cellulose nanofiber powder was purchased from Guilin Qihong Technology Co. (China). High-glucose Dulbecco's modified Eagle's medium (DMEM), fetal bovine serum (FBS, HyClone), penicillin/streptomycin, and other reagents for cell preparation were all purchased from GE Inc. (China). A live/dead staining kit (BB-4126) was purchased from BestBio Inc. (China). An alamar blue assay kit

Table 1: Proportion of ingredients in the tested hydrogels.

Group	Abbreviation	Gelatin	Alginate	CNF
1	HGA-CNF	20% (*w*/*v*)	1.25% (*w*/*v*)	0.25% (*w*/*v*)
2	HGA	20% (*w*/*v*)	1.25% (*w*/*v*)	—
3	LGA-CNF	10% (*w*/*v*)	1.25% (*w*/*v*)	0.25% (*w*/*v*)
4	LGA	10% (*w*/*v*)	1.25% (*w*/*v*)	—

(A7631) was purchased from Solarbio Inc. An immunohistochemistry tool kit (SP-0023), rabbit monoclonal primary antibodies for collagen type I (BS-10423R 1 : 400, 1 mg mL^{-1}), collagen type II (BS-10589R, 1 : 100, 1 mL mL^{-1}), and collagen type X (BS-0554R, 1 : 200, 1.4 mg mL^{-1}) were purchased from Bioss Inc. (China).

2.2. Preparation of Bioinks. CNF powder was diluted in deionized water to a final concentration of 0.25 wt% through stirring at 1000 rpm for 30 min at room temperature to acquire a homogenous solution. The solution was then heated to 70°C, and the Na-alginate powder was added under magnetic stirring for 30 min. Gelatin powder was added and dissolved when the solution was cooled to approximately 50°C under magnetic stirring for another 30 min. NaOH was used to adjust the pH of the solution to approximately 7.5. The hydrogel solution was then placed in a constant temperature oscillator at 200 rpm and 37°C overnight to eliminate bubbles and maintain a homogenous mixture. The bioink was prepared on a clean bench, and all the components and equipment were autoclaved and/or sterilized using UV light. After the preparation was finished, the final hydrogel was heated to 100°C for 1 h and then sealed to keep it sterile. The bioink was stored at 4°C and heated to 37°C for 30 min in a water bath before the bioprinting process. To verify the printability and biocompatibility of the bioinks, six groups of hydrogels were prepared with varying concentrations of gelatin and CNF. To simplify the narration, hydrogels containing higher and lower content of gelatin were recorded as high-gelatin-containing alginate group (HGA) and low-gelatin-containing alginate group (LGA), respectively. The CNF-modified hydrogels were named as HGA-CNF and LGA-CNF, respectively (Table 1).

2.3. Rheological Characterization. The rheological analysis was performed using an MCR 702 rheometer (AtonParr, Austria) using a 25 mm parallel plate. All 4 groups of cell-free bioink samples were tested before and after cross-linking. 0.1% (*w*/*v*) $CaCl_2$ solution was used as a cross-linker. The cross-linking time was 1 min. The samples were store at 37°C before the test and heated to the experimental temperature for 5 min before the rheological measurements. Non-cross-linked hydrogels were characterized through flow and temperature sweeps. The flow sweeps were conducted to evaluate viscosity at a shear rate ranging from 0.1 to 100 s^{-1} at 25°C. To evaluate the thermal responsivity of the hydrogels, the viscosity was measured at temperatures ranging from 1°C to 40°C, at a fixed shear rate of 1 s^{-1}. The cross-linked hydrogels were characterized through oscillatory frequency sweeps between 0.1 and 10 Hz in the linear viscoelastic region of the hydrogels at 37°C.

2.4. Cell Preparation. Primary rabbit fibrochondrocytes (rFCs) were used in bioprinting the cell-laden meniscal prototypes. The isolation and culture of rFCs have been described by previous studies [24]. Briefly, sequential treatment of finely diced meniscus (from 6-month-old rabbits) using 0.5% hyaluronidase, 0.2% trypsin, and 0.2% collagenase was applied to obtain the cells. Then, the cells were filtered through a fine nylon mesh to separate them from undigested tissue and debris. The filtrate was washed several times through gentle suspension in D-Hank's solution and underwent centrifugation at low speed ($1000 \times g$) to form a cell pellet. The cells were then cultured under conventional conditions at 37°C in a humidified atmosphere of 5% CO_2. Once a sufficient cell quantity was achieved, usually after the third or fourth passage, the cells were used for further bioprinting process.

2.5. Design of Microextrusion Bioprinter. In the current study, a microextrusion-based bioprinter (BP-1) was developed by our group. The minimum mechanical travel distance is ±0.05 mm for the *XY*-axes and ±0.01 mm for the *Z*-axis. The extrusion module was consisting of a precision piston for extruding materials, a syringe heater for thinning printing materials, and a standard medical syringe (10 mL) as a cartridge with 22G metal nozzles for depositing bioinks. The whole printing system is enclosed by a clean bench with a temperature-humidity control system. A UV light source was also integrated for sterilization. In a typical print procedure, the *XY* stage will translate the extruder at speeds ranging from 1 mm/s to 10 mm/s to pattern the predetermined 2D cross-section on the printing substrate, and then the *Z* stage elevates to repeat the process for the next layer. Special methods were applied to ensure the sterilization of the whole bioprinting system. Firstly, the whole bioprinter was installed in a modified super clean bench which was divided into two separate cabins by a plate. The mechanical structures of the bioprinter were in the upper cabin where the bioprinting process was carried out and the control system was installed in the cabin below. All cables in the upper cabin were waterproof. Secondly, before the bioprinting process, thorough disinfection by alcohol spray and UV irradiation was carried out in the upper cabin for 40 min. At last, the super clean bench was kept closed the positive pressure during the bioprinting process.

2.6. Printability Verification Process. The bioinks were heated in a water bath at 37°C for 30 min and extracted into a standard sterile syringe with 22G (0.42 mm inner diameter) metal needles. The samples were printed directly onto sterile Petri dishes on the printing platform, which was cooled down to 4°C by the printing platform during the process. Square blocks (15 mm × 15 mm × 2 mm) consisting of four perpendicular layers with a 40% filling rate were 3D printed. Considering the nonlinear rheological performance of living cells, the samples used for printability tests were cell-free to reduce disturbance. The printing temperature range was

Table 2: MRI parameters for knee scanning.

FOV, mm	Matrices	TR, ms	TE, ms	Slice thickness, mm
180 × 180	320 × 320	1500	32	0.8
Bandwidth, kHz	Echo train length	NEX	Scan time, mins	
83.33	60	1	6.29	

FOV: field of view; TR: repetition; TE: echo time; NEX: number of excitations.

20°C–25°C. The best printing temperature was decided on the base of the actual filamentation of each group under a certain temperature. The platform temperature for all groups was set to 4°C. The moving speed of the nozzle in XY-axes was 3 mm/s. All samples were cross-linked immediately using 0.1% w/v $CaCl_2$ for 1 min and then washed twice using Dulbecco's phosphate-buffered saline (DPBS).

2.7. Patient's Specific Design of Meniscal Prototype. To mimic the native shape of the meniscus, a 3D model of the medial meniscus was achieved based on MRI scans from one healthy volunteer of the authors. MRI images were acquired through the 3Tesla Discovery MR750 GEM Magnetic Resonance Imaging System (GE Healthcare, United Kingdom) with a 16-element phased-array flexible coil. A general supine position with a relaxed limb was used when performing the scan. Sagittal 3D fast-spin-echo (FSE) with high spatial, contrast resolution and no chem SAT was applied for image achievement. MRI scan parameters for the knee imaging are listed in Table 2.

The MRI data were saved as a sequence of Digital Imaging and Communications in Medicine (DICOM) files and processed via the Mimics software (Materialise 21, Belgium). The threshold was set to 50-200 GV to identify meniscal tissues from surrounding tissues. The model was then carefully trimmed artificially by an experienced orthopedic surgeon to reconstruct the morphology of the medial meniscus. After that, an automatic adjustment was applied to fill the cavities caused by signal noise and exported as an STL file. The STL model was then converted to a motion program (G-code) using an open-source software (Repetier-Host, Germany), which describes the operation of the dispensing nozzles, printing speed, nozzle heat, and other relative information. A different open-source software (Printrun, by Kliment Yanev) was applied to transfer the G-code files into the operating computer for bioprinting.

2.8. Bioprinting Process. After the printability verification process, HGA-CNF was selected as the bioink used for further bioprinting tests. Centrifuged rFCs were resuspended with 5 mL liquefied HGA-CNF directly. The cell number of the resuspension solution was 5×10^6. Slight oscillation of the mixed bioink was performed for 10 min at 37°C to homogenize the solution. The cell-laden bioinks were extracted into syringes with 22G (0.42 mm inner diameter) metal needles. To eliminate the bubbles in the bioinks, all syringes were settled in the incubator at 37°C for 20 min. The bioprinting process was conducted with BP-1, and the structures were printed directly onto sterile Petri dishes on the printing platform, which was cooled down to 4°C during the process.Since it has been reported that cellular activities would be compromised when encapsulated into solidly structured hydrogel scaffolds [25, 26]. To improve the nutrition exchange inside the hydrogel-based scaffolds, all structures were designed based on the lattice structure. The printing temperature was 25°C. The platform temperature was set to 4°C. The 3D-reconstructed meniscus model with a 40% filling rate and rectilinear filling patterned was bioprinted. The printing speed was 3 mm/s. All samples were cross-linked immediately after bioprinting using 0.1% w/v $CaCl_2$ for 1 min. To simplify the process, cell-laden, square block samples were bioprinted for metabolic activity test. The bioprinted samples were cultured in a petri dish ($\varphi = 55$ mm) and incubated for 14 days. The medium was changed every 3 d.

2.9. Printability Evaluation and Characterization. The printing quality was evaluated by imaging the cross-linked cell-free samples using a ×4 air objective with an SZX16 stereoscopic microscope (OLYMPUS, Japan), and bioinks from all groups were used in this test. Briefly, cross-linked cell-free structures with four layers were imaged to measure the strand width and pore size using the ImageJ software. The spreading ratio was calculated by dividing the strand width by the inter diameter (22G, ~420 μm) of the nozzle. The printed structures were stained using trypan blue after printing for better visualization. Scanning electron microscopy (SEM, Zeiss EVO 18, Cambridge, England) was applied to further characterize the porosity and interconnectivity of the bioprinted samples. The samples were lyophilized and sputter-coated with gold to observe the topography. Images (×25 and ×1500) were taken using SEM at an accelerating voltage of 3 kV to evaluate the morphology and microarchitectures. Three random images were taken from each sample from every region. To better visualize the rFCs encapsulated inside the structures, three samples were first graded ethanol dehydrated and then went through the same processes as other samples.

2.10. Cell Viability and Metabolic Activity. The cell viability of cells in the bioprinted structures was qualitatively analyzed at day 1, as well as 4, 7, and 14 d of culture using a live/dead staining kit in accordance with the manufacturer's instructions. Briefly, the bioprinted structures were rinsed using DPBS twice and incubated in 5 mL of live/dead solution (calcein-AM and ethidium homodimer) at 4°C for 20 min. The samples were examined using a fluorescence microscope (Zeiss, Axio Imager 2, Germany). Five randomly selected images obtained at ×4 magnification were used to evaluate the percentage of cell viability via ImageJ. The viability was calculated as the average ratio of live cells to total cells. An alamar blue assay kit was used to measure cell proliferation. The metabolic activity of the encapsulated cells was analyzed at 1, 4, 7, and 14 d after bioprinting. The square block bioprinted structures were incubated in 6-well plates for 7 h with 0.3 mL of alamar blue solution for each 3 mL of culture media. Fluorescence intensity was measured at an excitation

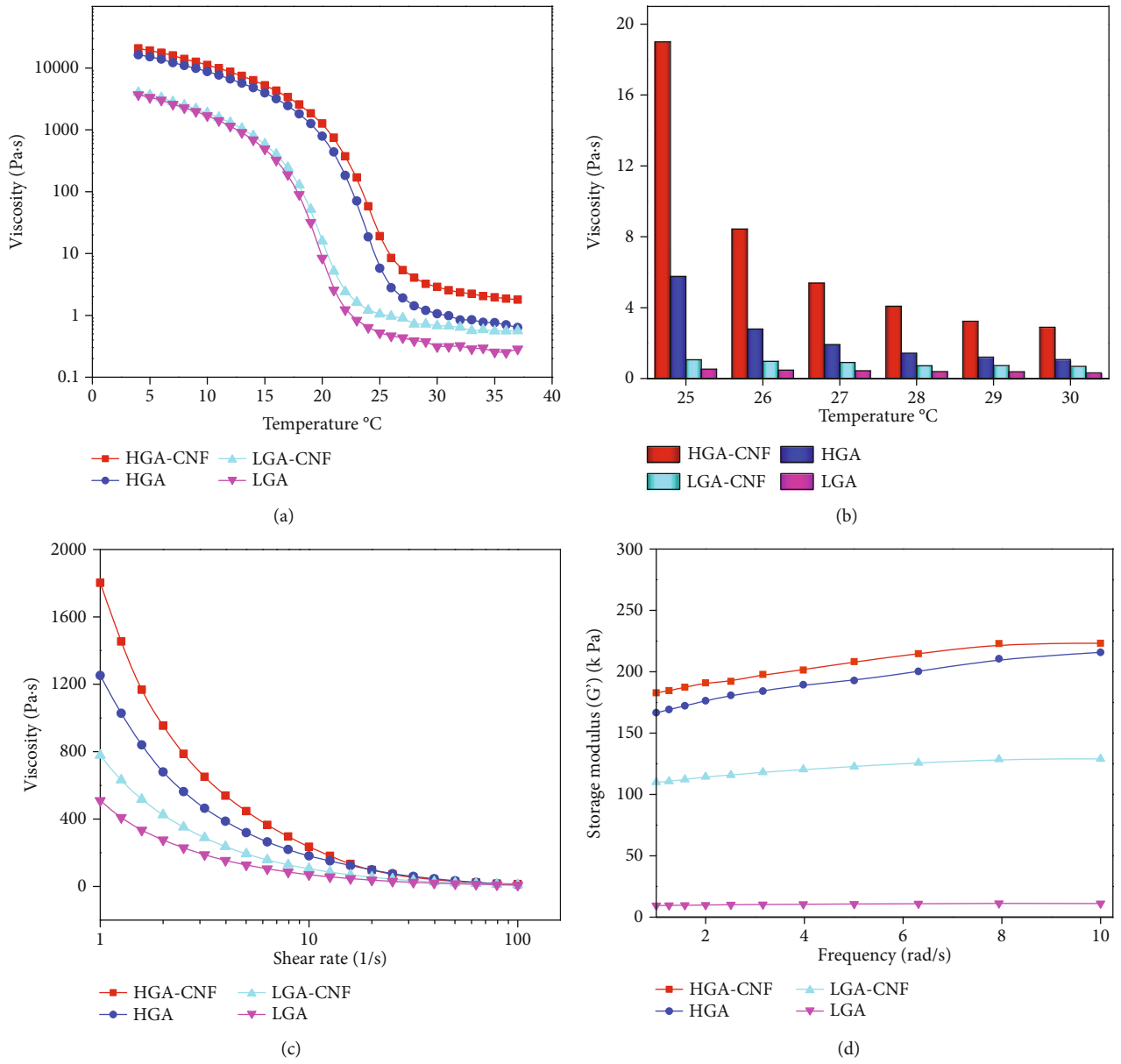

Figure 1: Rheological characterization of the cell-free hydrogels. (a) Viscosity at temperatures ranging from 5°C to 37°C at a shear rate of 1 s^{-1}. (b) Non-cross-linked viscosity at bioprinting temperature from 20°C to 25°C at a shear rate of 1 s^{-1}. (c) Non-cross-linked viscosity at various shear rates at 25°C. (d) Storage modulus after cross-linking at 37°C.

wavelength of 530 nm and an emission wavelength of 590 nm (Varioskan Flash, Thermo Fisher, USA).

2.11. Histology and Immunohistochemistry. The prototypes incubated for 14 d in the culture medium were fixed in paraformaldehyde/barium chloride overnight. The fixed samples were then cryosectioned, embedded in paraffin wax, sectioned at 5 μm, and affixed to microscope slides. Hematoxylin-eosin, picrosirius red, and alcian blue staining were applied to assess calcium, collagen, and glycosaminoglycan accumulation, respectively. Immunohistochemistry techniques were applied to evaluate and identify collagen types I, II, and X, as previously described [27]. Briefly, samples were treated using peroxidase and chondroitinase ABC and then incubated with fetal calf serum to reduce nonspecific binding. Collagen type I, collagen type II, and collagen type X rabbit monoclonal primary antibodies were applied for 1 h at room temperature. The secondary antibody (anti-rabbit IgG biotin conjugate) was added for 1 h, followed by incubation with an ABC reagent for 45 min. Finally, sections were developed using DAB peroxidase for 5 min.

2.12. Statistical Analysis. Results are expressed as mean ± standard deviation. Statistical analyses were performed using the SPSS v22.0 software (SPSS Inc., Chicago, IL, USA).

3. Results

The rheological behavior is considered as the major concern to select the bioink candidate for further bioprinting tests. All

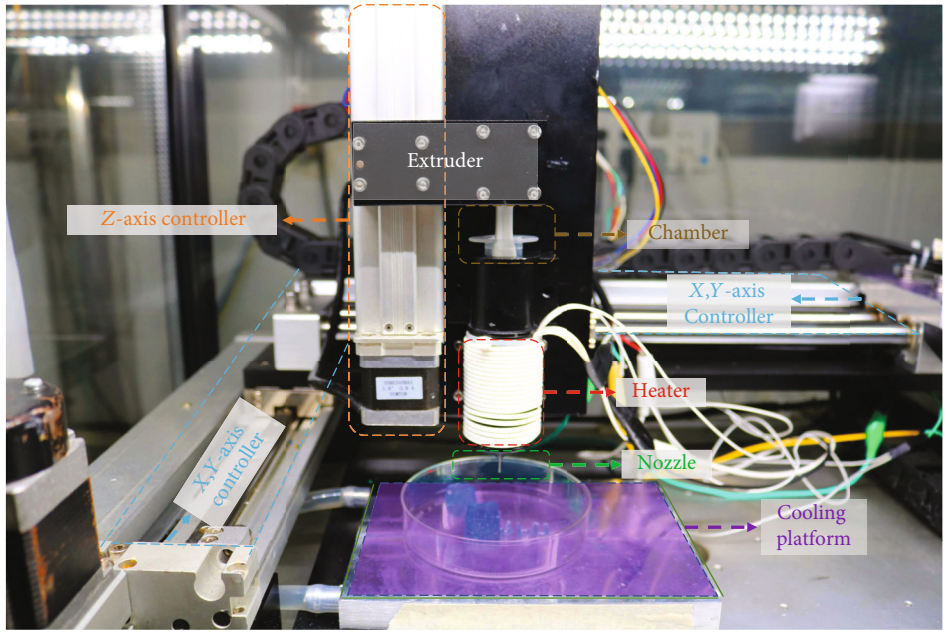

Figure 2: Microextrusion-based bioprinter developed by our group.

four groups of prepared hydrogels with varying gelatin and CNF content were tested (Figure 1). The samples showed a significant decrease in viscosity as the temperature increased during a temperature sweep (Figure 1(a)). Hydrogels containing a higher concentration of gelatin (20% *w*/*v*) maintained higher viscosity among all the groups when the temperature raised to 25°C, which is the minimum acceptable printing temperature for the bioprinter. CNF-modified hydrogels exhibit prior viscosities and lower decreasing rates than their non-CNF-containing counterparts. At the designated bioprinting temperature window of 25°C to 30°C, HGA-CNF exhibited more than a threefold increase in viscosity compared with HGA (Figure 1(b)), indicating prominent superiority in printability potential. A shear-thinning behavior was observed among all the bioink candidates. As CNF strengthened the viscosity, hydrogels modified with CNF tended to maintain more solid-like behaviors than non-CNF-containing hydrogels at the same shear rate (Figure 1(c)). The frequency sweep also showed a similar tendency, and hydrogels modified with CNF showed higher storage modulus than pure gelatin with alginate when being cross-linked by Ca^{2+}, indicating priority in the mechanical performance of CNF-modified samples (Figure 1(d)).

Printability is the vital access to maintain the fidelity of the meniscal prototype. Cell-free square block samples and rFCs cell-laden meniscal prototypes were printed using our microextrusion-based bioprinter (Figure 2). The quality assessments and characterization of the printed structures are presented in Figure 3. To acquire better printing filamentation, all the hydrogels were tested under a printing temperature range from 20°C to 25°C, which was decided based on the rheological results of the hydrogels (Figure 3(a)). HGA-CNF and HGA showed the best filamentation under 25°C while the highest acceptable printing temperature for LGA-CNF and LGA was 20°C. The other printing parameters remained the same for all hydrogels. Top-view images are presented in Figure 3(b). The results showed that only HGA-CNF and HGA formed 3D lattice structures with relatively acceptable fidelity and integrity. Samples bioprinted with LGA showed completely fused constructs during the test. Thus, the measurement of the filament was not performed for LGA. To analyze the bioprinted samples in more detail, stereomicroscope images of the top layers were taken. The strand width and pore size were measured (Figures 3(c) and 3(d)). The spreading ratios of HGA-CNF, HGA, and LGA-CNF were 0.88 ± 0.08, 1.07 ± 0.03, and 1.03 ± 0.07, respectively. The strands of the CNF-modified hydrogels (HGA-CNF and LGA-CNF) were stretched at different levels during the printing process, which led to a thinner strand width than their non-CNF-containing counterparts. The pore size measurement further confirmed this feature. The presence of CNF resulted in a thinner strand width and better lattice formation in the printed structures. Structural investigations of the printed structures of cell-laden HGA-CNF via scanning electron microscopy (SEM) are presented in Figure 3(e). Hierarchical porous structures of micron order were observed, presenting a similar microenvironment to the morphological features of the extracellular matrix (ECM). The sign of cellular component in the bioink was more distinct after treating the samples with graded ethanol dehydration. The bioink scaffold and rFCs encapsulated inside were colored as green and fuchsia, respectively, for better visualization. Homogeneous distribution of rFCs within the hydrogel-based scaffolds was observed, indicating the biocompatibility of our bioprinting process. In summary, good printability of HGA-CNF was demonstrated, and this was then selected as a bioink for further bioprinting tests.

The anatomical features of the meniscus extracted from the 2D MRI images were preserved and reshaped as 3D

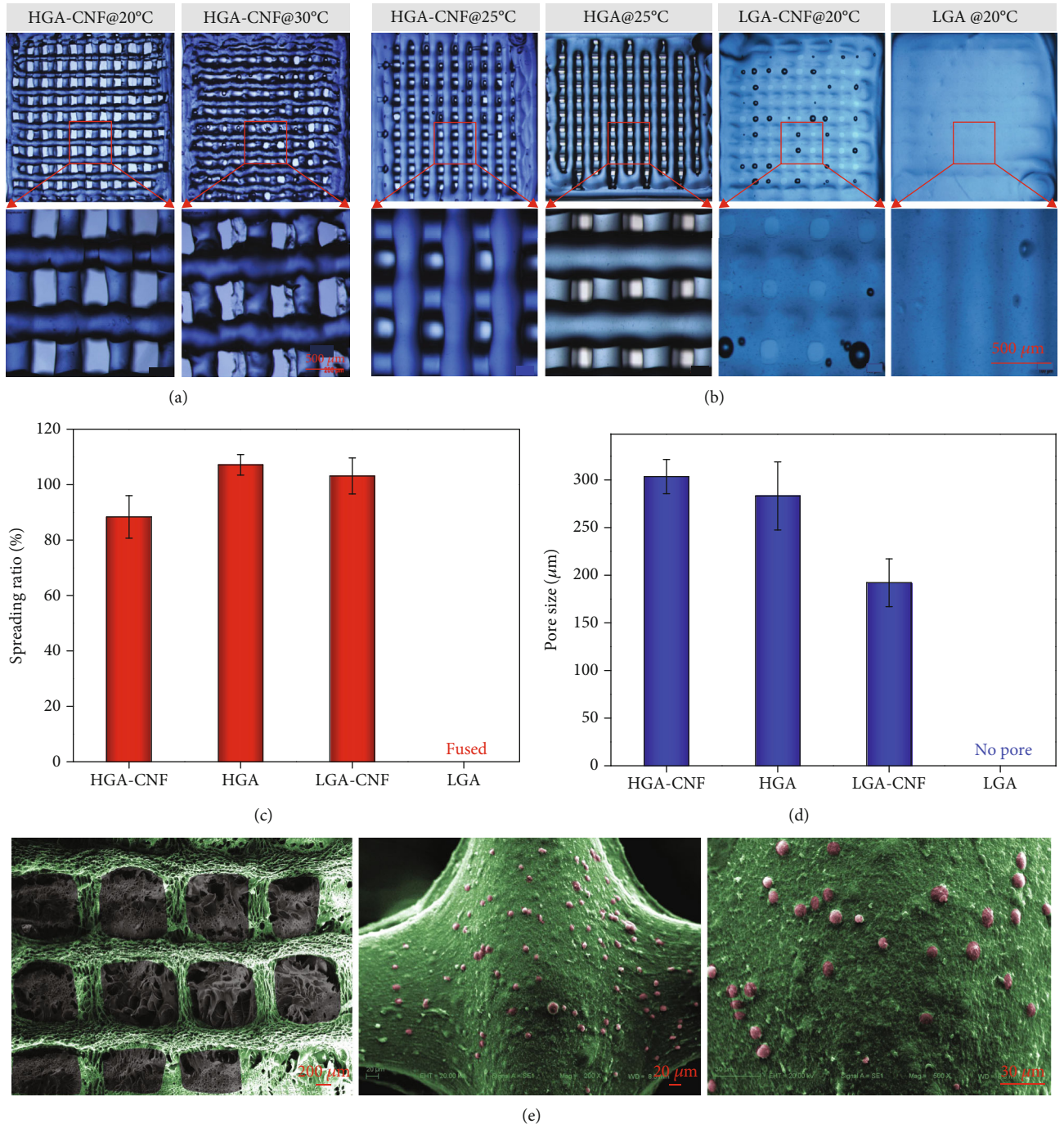

Figure 3: Bioprinting quality assessment. (a) As the printing temperature raise, gelling properties from over extrusion (30°C) and poor gelling (20°C) of the bioinks were observed. (b) Upper row: top-view images of the printed four-layer structures (trypan blue stained, cross-linked) obtained using a stereoscopic microscope. (c) The spreading ratios of the non-cross-linked fourth layer strands were measured. (d) The pore sizes of the non-cross-linked four-layer structures were measured. (e) SEM analysis of the printed structures. The bioink and rFCs are colored green and fuchsia, respectively.

volumetric information and then bioprinted into a hydrogel-based, cell-laden meniscal prototype (Figure 4). The selected bioink (HGA-CNF) presented good printability and shape fidelity during the printing process. The 3D-printed meniscus prototype was consisting of 19 layers, consuming approximately 991.85 mm^3 volume of bioink. The actual size of the printed meniscus prototype was approximately $48.3 \times 40.5 \times 8.28$ mm before cross-linking, while the designed shape of the 3D model reconstructed from MRI date was $45.42 \times 41.13 \times 8.81$ mm, indicating highly consistency.

The viability and metabolic activity of rFCs in the printed samples are presented in Figure 5. The results showed very high viability after the bioprinting process in a live/dead staining assay (Figure 5(a)). In detail, the average cell viability

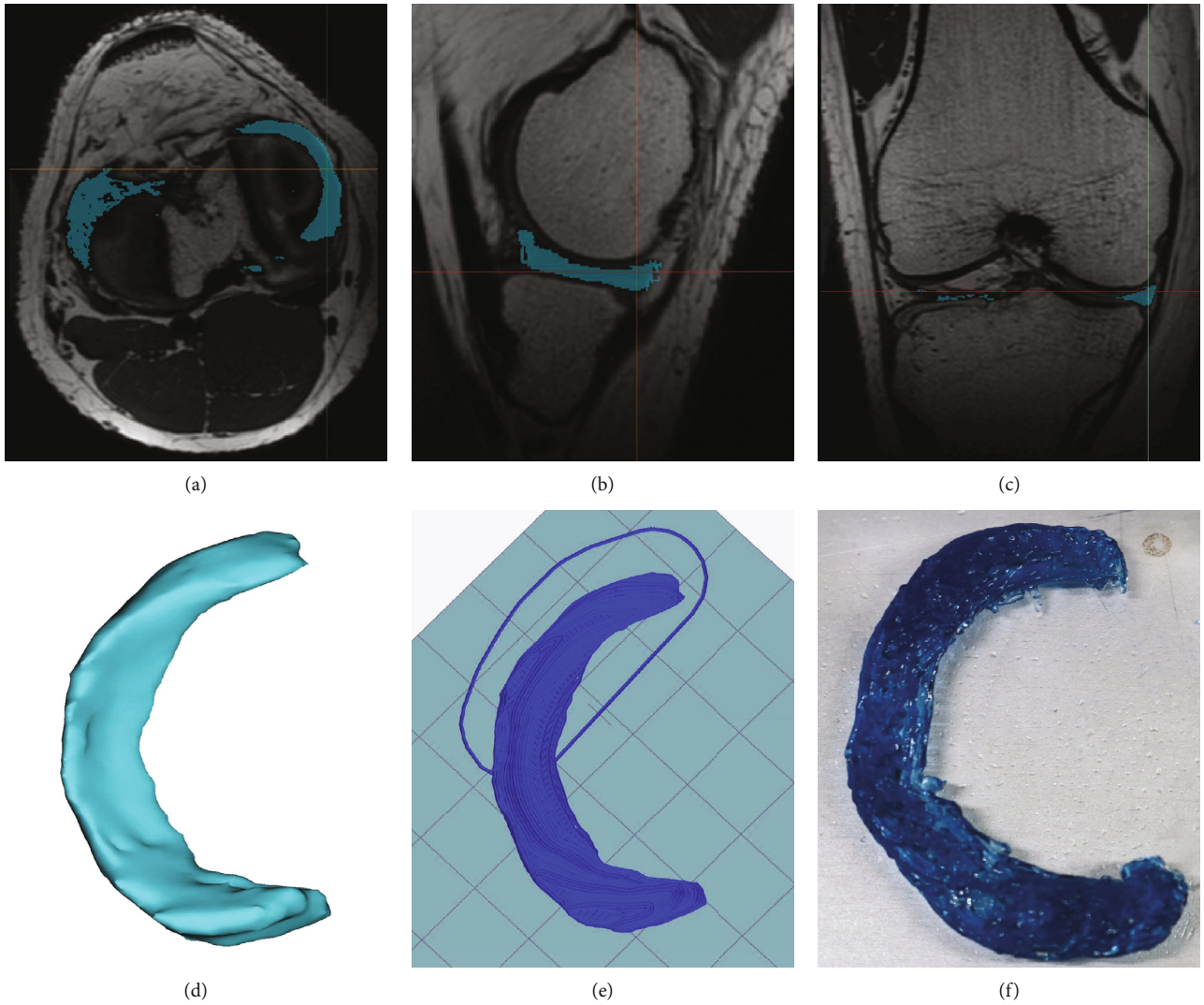

Figure 4: 3D reconstruction from MRI images and 3D printing process of a patient's specific medial meniscus. (a–c) MRI data gathered from a healthy volunteer were processed to identify the structure of medial meniscus. (d) A 3D model was then reconstructed and converted to STL file. (e) The STL model was imported into the slicing software to calculate the printing route and a G-code file was generated. (f) Bioink-based, cell-free meniscal prototype was then 3D printed basing on the G-code file.

of the rFCs on day 1 was $94 \pm 0.03\%$. However, the bioprinted cells recovered from the printing shock within 4 d of culture ($95 \pm 0.05\%$) and retained high performance throughout the culture period. When it came to day 7, the viability of the rFCs reached a peak of nearly 99% and then dropped to $96 \pm 0.02\%$ for the following 7 d of culture, demonstrating the excellent biocompatibility of HGA-CNF (Figure 5(b)). The alamar blue assay of the bioprinted rFCs (Figure 5(c)) was in line with the viability results. The metabolic activity of the printed cells was initially hampered by the bioprinting process and then recovered to a significantly high level at 4 d after bioprinting, indicating high cell proliferation activity during the first few days. The metabolic activity decreased gradually between 4 and 7 d of culture and stabilized at day 14.

To ascertain the deposition of collagen and sGAG in vitro, bioprinted samples encapsulating rFCs were histologically stained after 14 d of incubation (Figure 6(a)). Picrosirius red and alcian blue staining was positive in the intercellular space of rFCs encapsulated in the bioprinted samples, indicating collagen and glycosaminoglycans accumulation. HE staining of the bioprinted structures revealed rFCs were homogeneously distributed in the bioink. Immunohistochemical staining showed barely signs of collagen type I and abundant accumulation of collagen types II and X (Figure 6(b)).

4. Discussion

To meet the growing demand for meniscus tissue engineering, both synthetically and naturally derived biomaterials have been reported [28]. However, although it has been reported that shape mismatch can lead to a negative influence on the biomechanical performance of implanted meniscus [29, 30], the morphological design of the meniscus and development of relative fabrication approaches were unvalued to some

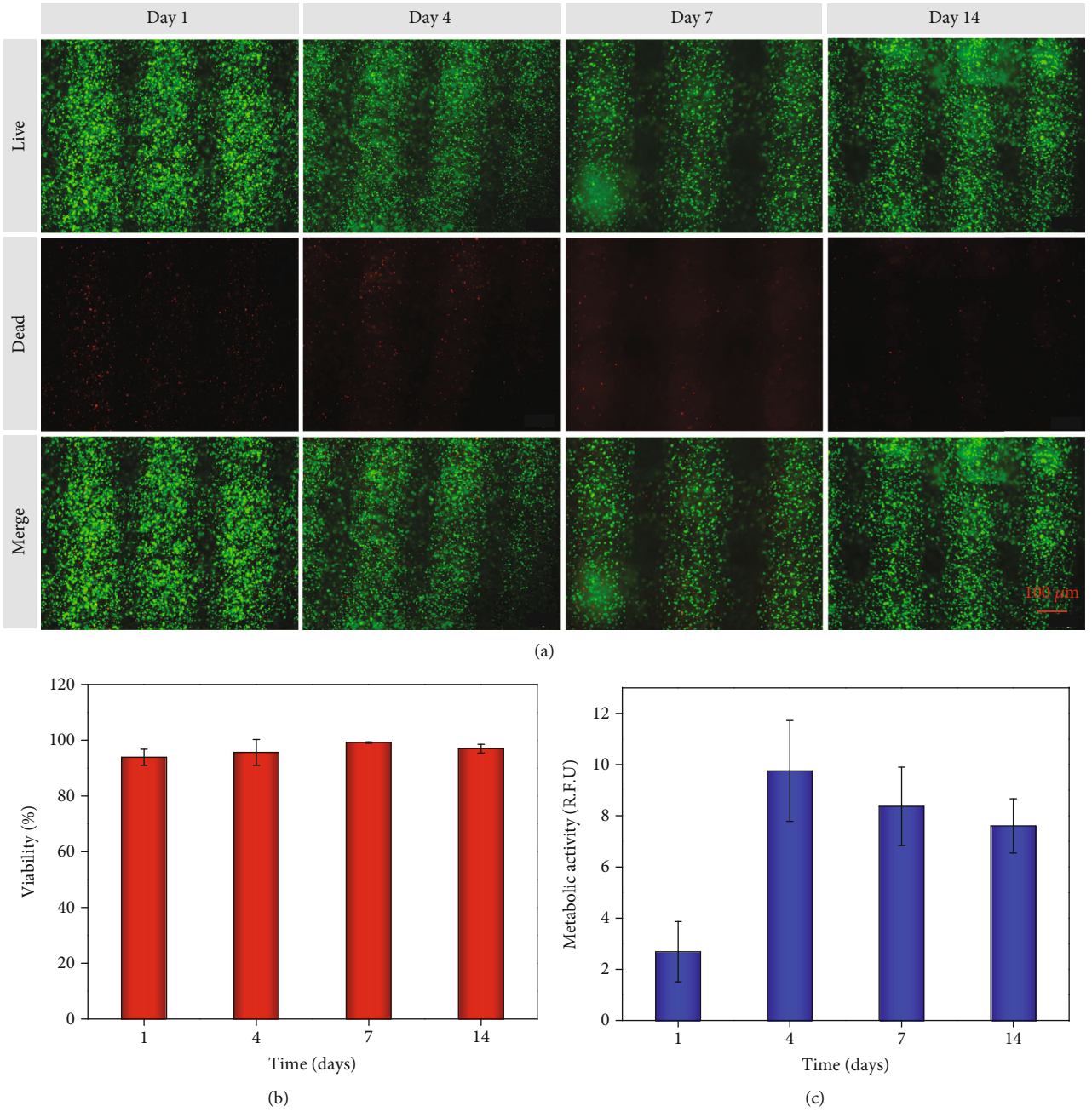

Figure 5: Viability and metabolic activity of bioprinted samples. (a) Live/dead staining of rFCs immediately at 1, 4, 7, and 14 d of culturing in vitro. Living cells are stained green and dead cells red. Scale bar 100 μm. (b) Quantitative statistics of the bioprinted samples at different time points using ImageJ. (c) Metabolic activity values of bioprinted rFCs using an alamar blue assay at different time points.

extent. To address this situation, the precise morphological design was stressed in this study. A 3D-reconstructed model was achieved from the patient's MRI images, aiming at accurately revealing the native shape parameters of the meniscus. During the MRI scanning, modified parameters were applied to acquire better accuracy. Generally, OAx fs PD, OSag fs PD, and OCor fs PD models were used for a meniscal scan while our scan was a combination of these three models with a thinner slice thickness. The time consuming for a general meniscal MRI scan was approximately 5.23 min while our modified model was 6.29 min. The modified parameters were prestored in the MRI device and could be readily switched as needed. Neither additional equipment nor extra economic cost was needed for the modified scan. Moreover, with the assistance of the 3D reconstruction software like Mimics, the meniscal model could also be achieved via mirroring the healthy side MRI data of the patient when the major substance of injured meniscus has been damaged. As for partial meniscal injure cases, a mirroring of the healthy side MRI data could be used as a reference. The injured area could be underlined via a matching between the healthy and injured meniscus.

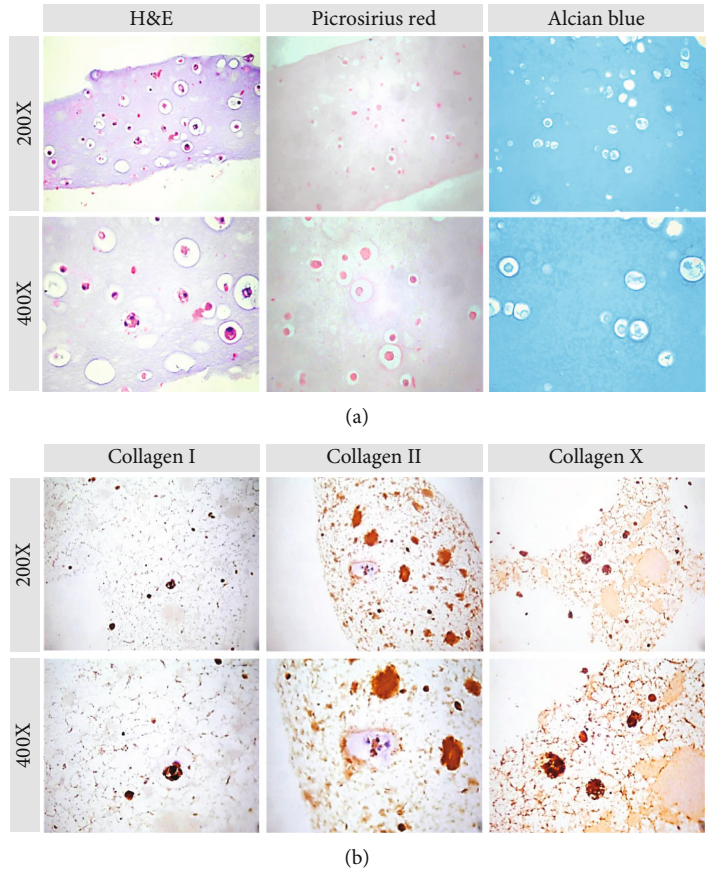

FIGURE 6: Histological and immunohistochemical results of bioprinted structures. (a) Histological staining of bioprinted rFCs structures with HE, picrosirius red, and alcian blue. (b) Immunohistochemical for collagen I, II, and X accumulation in the bioprinted rFCs samples.

Benefitting from a bottom-up style of manufacturing and precise cell patterning, bioprinting is naturally suitable for biofabricating tissue engineering scaffolds with complex structures. In this process, the balance between printability and biocompatibility has been a major challenge since the early development of bioinks. In this context, a microextrusion-based bioprinting system was built by the current research group to explore its potential of personalized-designed meniscal reconstruction. Gelatin-alginate-based bioink was adapted to achieve thermoresponsive and calcium ions cross-linking gelling features [31]. However, the thermal curing of gelatin is unstable and reversible during bioprinting, which commonly leads to inferior printability and fidelity when fabricating complex structures. Thus, maintaining a self-supporting hydrogel before ionic cross-linking is also an attractive feature that would improve printability.

The rheological characterization of the prepared hydrogels further confirmed the influence of CNF. Hydrogels containing CNF showed prior viscosity performance than their non-CNF-containing counterparts at a wide range of temperatures. This phenomenon could be attributed to the physicochemical interaction between CNF, alginate, and gelatin. It has been reported that hydroxyl surface groups exist in CNF and alginate can interact through hydrogen formation with carbonyl and amine groups in gelatin [32], improving the gelling strengthen of the hydrogel. Moreover, the existence of CNF also significantly improved the shear-thin behaviors of the hydrogels via the breakage of fiber networks under shear force [33]. In addition, nanofibers of CNF underwent shear-induced alignment from the nozzle, which further enhanced the bioink flow [34], resulting in better printability. The role of CNF in the bioink is a "booster" for both the extrusion and curing process through enhancing the shear-thinning behavior. During the extrusion process, the extrusion flow through the nozzle was enhanced by CNF via shear-induced fibril alignment, which results in a smoother and more continuous flow out of the nozzle. When the gelatin had undergone gelation, the CNF material present resulted in relatively high stiffness and self-supporting features through the formation of a self-aligned fibrous network scaffold which served as a stiff filler with favorable shear-thinning properties [35]. To enhance the printability of gelatin-alginate bioink, 0.25% *w*/*v* CNF was added in the current study. The bioprinted meniscus prototype can maintain shape fidelity without being instantly cross-linked.

Origin from natural resources, the biocompatibility of gelation and alginate has been verified [36]. As for CNF, although it is not degradable inside the human body, it has been reported that owing to the small size and inertness of CNF, the newly formed matrix simply surrounds the fibers and integrates them into the tissue without any adverse side effects [37]. The density value of CNF in this study is

therefore decided based on the reported studies [32]. The cytocompatibility of CNF-modified bioink, with a concentration of 0.25 mg/mL of CNF, was confirmed after the bioprinting process and additional incubation for 14 d. Our results showed that the bioprinted structures encapsulating rFCs allowed acceptable cell viability. Moreover, a structural investigation through SEM confirmed a multiscale interconnected porous morphology in the bioprinted structures, which could provide a suitable 3D environment for cell attachment, proliferation, and metabolism [38]. The metabolic activity that showed the bioactivities of rFCs were tiny compromised and quickly recovered after 4 days of incubation.

In this research, we used fibrochondrocytes to verify the ability bioprinting meniscal relevant cellular components of our system. Although applying stem cells in meniscal reconstruction has been reported by some groups. However, complex-staged-inducing methods were required for stem cells in fibrocartilaginous differentiation, consuming a relatively long period of cell culture which compromised the clinical potential [39]. Thus, mature cells were preferred by our group. Nevertheless, as the progress of coculturing stem cells with other meniscal relevant cells such as fibrochondrocytes and chondrocytes in 3D environments are reported recently [40, 41], further experiments on bioprinting mixed cell groups to enhance the proliferation and differentiation will be carried out by our group.

To further assess the ECM accumulation of fibrochondrocytes, sGAG and collagen types II and X were confirmed by histological and immunohistochemical tests simultaneously. The results showed the ECM components were similar to the native meniscus. This progress will pave the way towards the reconstruction of the patient's specific-designed, bioactive meniscal substitution. Moreover, to the best of our knowledge, this is the first time that primary fibrochondrocytes have survived through the bioprinting process and maintained viability and biofunction during further in vitro incubation. The bioprinted meniscal prototype would bring more flexible, adaptable, and easily accessible methods in meniscal repairment and reconstruction.

However, the current study still has some limitations. Firstly, further biomechanical tests of cell-laden meniscal prototypes are still needed to evaluate the in vitro mechanical performance. Considering the inferior mechanical properties of hydrogel-based bioinks, to further improve the mechanical performance of the meniscal prototype, coprinting of thermoplastic polymer and bioink would be our further direction [11]. Benefiting from the highly scalable of our bioprinter, the modification would be easily accessed. Moreover, in vivo implantation on animal models should be carried out further to verify the tissue formation abilities of our bioprinted prototypes. We predict that biofabrication of cell-laden meniscus prototype with proper biomechanical features meeting the clinical implantation demands would not be a barrier as the advance of bioprinting and biomaterial approaches.

5. Conclusions

The CNF-modified gelatin-alginate bioink has achieved encouraging results in mechanical performance and printability. Combining with MRI 3D reconstruction, the preliminary attempt of applying modified bioink in bioprinting individual-specific meniscus prototype is achieved with favorable biofunction. The application of bioprinting approaches might minimize the mismatch between artificial meniscal implants and native knee joint tissues, thereby permitting the evolution of clinical therapeutic methods of meniscal reconstruction.

Data Availability

The data used to support the findings of this study are available from the corresponding author upon request.

Conflicts of Interest

The funders had no role in the design of the study; in the collection, analyses, or interpretation of data; in the writing of the manuscript; or in the decision to publish the results.

Authors' Contributions

Conceptualization was done by Wenbin Luo and Zhengyi Song; methodology by Wenbin Luo; formal analysis by Wenbin Luo and Zhenguo Wang; investigation by Zuhao Li and Chenyu Wang; resources by He Liu; data curation by Jincheng Wang and Qingping Liu; writing original draft preparation by Wenbin Luo; visualization by He Liu and Qingping Liu; supervision by Jincheng Wang and Qingping Liu; project administration by Jincheng Wang and Qingping Liu. All authors have read and agreed to the published version of the manuscript.

Acknowledgments

This study was supported by the National Natural Science Foundation of China (grant no. 81671804 and 81772456), Scientific Development Program of Jilin Province (grant no. 20190304123YY, 20180623050TC, and 20180201041SF), Program of Jilin Provincial Health Department (grant no. 2019SCZT001 and 2019SRCJ001), Cultivation Program from the Second Hospital of Jilin University for National Natural Science Foundation (grant no. KYPY2018-01), and Youth Talents Promotion Project of Jilin Province (grant no. 192004), and Jilin Province Key Scientific and Technological Project (no. 20170204061GX).

Supplementary Materials

Supplementary 1. Video S1: bioprinting process of the meniscal prototypes.

Supplementary 2. Video S2: bioprinting process of the square block samples.

References

[1] A. Heijink, A. H. Gomoll, H. Madry et al., "Biomechanical considerations in the pathogenesis of osteoarthritis of the knee," *Knee Surgery, Sports Traumatology, Arthroscopy*, vol. 20, no. 3, article 1818, pp. 423–435, 2012.

[2] S. J. Lee, K. J. Aadalen, P. Malaviya et al., "Tibiofemoral contact mechanics after serial medial meniscectomies in the human cadaveric knee," *The American Journal of Sports Medicine*, vol. 34, no. 8, pp. 1334–1344, 2006.

[3] N. A. Smith, N. Parsons, D. Wright et al., "A pilot randomized trial of meniscal allograft transplantation versus personalized physiotherapy for patients with a symptomatic meniscal deficient knee compartment," *The Bone & Joint Journal*, vol. 100-B, no. 1, pp. 56–63, 2018.

[4] P. Mickiewicz, M. Binkowski, H. Bursig, and Z. Wróbel, "Preservation and sterilization methods of the meniscal allografts: literature review," *Cell and Tissue Banking*, vol. 15, no. 3, pp. 307–317, 2014.

[5] K. R. Myers, N. A. Sgaglione, and A. D. Goodwillie, "Meniscal scaffolds," *The Journal of Knee Surgery*, vol. 27, no. 6, pp. 435–442, 2014.

[6] Y. S. Shin, H. N. Lee, H. B. Sim, H. J. Kim, and D. H. Lee, "Polyurethane meniscal scaffolds lead to better clinical outcomes but worse articular cartilage status and greater absolute meniscal extrusion," *Knee Surgery, Sports Traumatology, Arthroscopy*, vol. 26, no. 8, pp. 2227–2238, 2018.

[7] M. E. Baratz, F. H. Fu, and R. Mengato, "Meniscal tears: the effect of meniscectomy and of repair on intraarticular contact areas and stress in the human knee. A preliminary report," *The American Journal of Sports Medicine*, vol. 14, no. 4, pp. 270–275, 1986.

[8] Y. S. Zhang, K. Yue, J. Aleman et al., "3D bioprinting for tissue and organ fabrication," *Annals of Biomedical Engineering*, vol. 45, no. 1, pp. 148–163, 2017.

[9] G. Gao, Y. Huang, A. F. Schilling, K. Hubbell, and X. Cui, "Organ bioprinting: are we there yet," *Advanced Healthcare Materials*, vol. 7, no. 1, article 1701018, 2018.

[10] M. Touri, F. Kabirian, M. Saadati, S. Ramakrishna, and M. Mozafari, "Additive manufacturing of biomaterials– the evolution of rapid prototyping," *Advanced Engineering Materials*, vol. 21, no. 2, p. 1800511, 2019.

[11] W. Luo, H. Liu, C. Wang, Y. Qin, Q. Liu, and J. Wang, "Bioprinting of human musculoskeletal interface," *Advanced Engineering Materials*, vol. 21, no. 7, article 1900019, 2019.

[12] S. Romanazzo, S. Vedicherla, C. Moran, and D. J. Kelly, "Meniscus ECM-functionalised hydrogels containing infrapatellar fat pad-derived stem cells for bioprinting of regionally defined meniscal tissue," *Journal of Tissue Engineering and Regenerative Medicine*, vol. 12, no. 3, pp. e1826–e1835, 2018.

[13] K. Markstedt, A. Mantas, I. Tournier, H. Martínez Ávila, D. Hägg, and P. Gatenholm, "3D bioprinting human chondrocytes with nanocellulose-alginate bioink for cartilage tissue engineering applications," *Biomacromolecules*, vol. 16, no. 5, pp. 1489–1496, 2015.

[14] S. Bose, D. Ke, H. Sahasrabudhe, and A. Bandyopadhyay, "Additive manufacturing of biomaterials," *Progress in Materials Science*, vol. 93, pp. 45–111, 2017.

[15] C. Mandrycky, Z. Wang, K. Kim, and D. H. Kim, "3D bioprinting for engineering complex tissues," *Biotechnology Advances*, vol. 34, no. 4, pp. 422–434, 2016.

[16] H. A. Awad, M. Q. Wickham, H. A. Leddy, J. M. Gimble, and F. Guilak, "Chondrogenic differentiation of adipose-derived adult stem cells in agarose, alginate, and gelatin scaffolds," *Biomaterials*, vol. 25, no. 16, pp. 3211–3222, 2004.

[17] M. Hospodiuk, M. Dey, D. Sosnoski, and I. T. Ozbolat, "The bioink: a comprehensive review on bioprintable materials," *Biotechnology Advances*, vol. 35, no. 2, pp. 217–239, 2017.

[18] S. Wüst, M. E. Godla, R. Müller, and S. Hofmann, "Tunable hydrogel composite with two-step processing in combination with innovative hardware upgrade for cell-based three-dimensional bioprinting," *Acta Biomaterialia*, vol. 10, no. 2, pp. 630–640, 2014.

[19] M. Neufurth, X. Wang, H. C. Schröder et al., "Engineering a morphogenetically active hydrogel for bioprinting of bioartificial tissue derived from human osteoblast-like SaOS-2 cells," *Biomaterials*, vol. 35, no. 31, pp. 8810–8819, 2014.

[20] L. G. Bracaglia, B. T. Smith, E. Watson, N. Arumugasaamy, A. G. Mikos, and J. P. Fisher, "3D printing for the design and fabrication of polymer-based gradient scaffolds," *Acta Biomaterialia*, vol. 56, pp. 3–13, 2017.

[21] T. Saito, T. Uematsu, S. Kimura, T. Enomae, and A. Isogai, "Self-aligned integration of native cellulose nanofibrils towards producing diverse bulk materials," *Soft Matter*, vol. 7, no. 19, pp. 8804–8809, 2011.

[22] A. Rashad, K. Mustafa, E. B. Heggset, and K. Syverud, "Cytocompatibility of wood-derived cellulose nanofibril hydrogels with different surface chemistry," *Biomacromolecules*, vol. 18, no. 4, pp. 1238–1248, 2017.

[23] X. Li, J. Wei, K. E. Aifantis et al., "Current investigations into magnetic nanoparticles for biomedical applications," *Journal of Biomedical Materials Research Part A*, vol. 104, no. 5, pp. 1285–1296, 2016.

[24] M. S. Son and M. E. Levenston, "Quantitative tracking of passage and 3D culture effects on chondrocyte and fibrochondrocyte gene expression," *Journal of Tissue Engineering and Regenerative Medicine*, vol. 11, no. 4, pp. 1185–1194, 2017.

[25] K. Zhang, Y. Fan, N. Dunne, and X. Li, "Effect of microporosity on scaffolds for bone tissue engineering," *Regenerative Biomaterials*, vol. 5, no. 2, pp. 115–124, 2018.

[26] C. R. Pimentel, S. K. Ko, C. Caviglia et al., "Three-dimensional fabrication of thick and densely populated soft constructs with complex and actively perfused channel network," *Acta Biomaterialia*, vol. 65, pp. 174–184, 2018.

[27] E. Harris, Y. Liu, G. Cunniffe et al., "Biofabrication of soft tissue templates for engineering the bone-ligament interface," *Biotechnology and Bioengineering*, vol. 114, no. 10, pp. 2400–2411, 2017.

[28] L. Roseti, C. Cavallo, G. Desando et al., "Three-dimensional bioprinting of cartilage by the use of stem cells: a strategy to improve regeneration," *Materials*, vol. 11, no. 9, p. 1749, 2018.

[29] S. V. Sekaran, M. L. Hull, and S. M. Howell, "Nonanatomic location of the posterior horn of a medial meniscal autograft implanted in a cadaveric knee adversely affects the pressure distribution on the tibial plateau," *The American Journal of Sports Medicine*, vol. 30, no. 1, pp. 74–82, 2002.

[30] M. Dienst, P. E. Greis, B. J. Ellis, K. N. Bachus, and R. T. Burks, "Effect of lateral meniscal allograft sizing on contact mechanics of the lateral tibial plateau: an experimental study in human cadaveric knee joints," *The American Journal of Sports Medicine*, vol. 35, no. 1, pp. 34–42, 2007.

[31] Q. Gao, Y. He, J. Z. Fu, A. Liu, and L. Ma, "Coaxial nozzle-assisted 3D bioprinting with built-in microchannels for nutrients delivery," *Biomaterials*, vol. 61, pp. 203–215, 2015.

[32] K. Wang, K. C. Nune, and R. D. Misra, "The functional response of alginate-gelatin-nanocrystalline cellulose injectable hydrogels toward delivery of cells and bioactive molecules," *Acta Biomaterialia*, vol. 36, pp. 143–151, 2016.

[33] M. Ojansivu, A. Rashad, A. Ahlinder et al., "Wood-based nanocellulose and bioactive glass modified gelatin-alginate bioinks for 3D bioprinting of bone cells," *Biofabrication*, vol. 11, no. 3, article 035010, 2019.

[34] S. S. Athukoralalage, R. Balu, N. K. Dutta, and C. N. Roy, "3D bioprinted nanocellulose-based hydrogels for tissue engineering applications: a brief review," *Polymers*, vol. 11, no. 5, p. 898, 2019.

[35] A. S. Gladman, E. A. Matsumoto, R. G. Nuzzo, L. Mahadevan, and J. A. Lewis, "Biomimetic 4D printing," *Nature Materials*, vol. 15, no. 4, pp. 413–418, 2016.

[36] L. Benning, L. Gutzweiler, K. Tröndle et al., "Cytocompatibility testing of hydrogels toward bioprinting of mesenchymal stem cells," *Journal of Biomedical Materials Research Part A*, vol. 105, no. 12, pp. 3231–3241, 2017.

[37] M. Müller, E. Öztürk, Ø. Arlov, P. Gatenholm, and M. Zenobi-Wong, "Alginate sulfate-nanocellulose bioinks for cartilage bioprinting applications," *Annals of Biomedical Engineering*, vol. 45, no. 1, pp. 210–223, 2017.

[38] A. G. Tabriz, M. A. Hermida, N. R. Leslie, and W. Shu, "Three-dimensional bioprinting of complex cell laden alginate hydrogel structures," *Biofabrication*, vol. 7, no. 4, article 045012, 2015.

[39] C. H. Lee, S. A. Rodeo, L. A. Fortier, C. Lu, C. Erisken, and J. J. Mao, "Protein-releasing polymeric scaffolds induce fibrochondrocytic differentiation of endogenous cells for knee meniscus regeneration in sheep," *Science Translational Medicine*, vol. 6, no. 266, p. 266ra171, 2014.

[40] L. Moradi, M. Vasei, M. M. Dehghan, M. Majidi, S. Farzad Mohajeri, and S. Bonakdar, "Regeneration of meniscus tissue using adipose mesenchymal stem cells-chondrocytes co-culture on a hybrid scaffold: in vivo study," *Biomaterials*, vol. 126, pp. 18–30, 2017.

[41] M. C. McCorry, J. L. Puetzer, and L. J. Bonassar, "Characterization of mesenchymal stem cells and fibrochondrocytes in three-dimensional co-culture: analysis of cell shape, matrix production, and mechanical performance," *Stem Cell Research & Therapy*, vol. 7, no. 1, p. 39, 2016.